Entropy Wave Instability in Dirac and Weyl Semimetals

P. O. Sukhachov,[1,*] E. V. Gorbar,[2,3] and I. A. Shovkovy[4,5]

[1] *Department of Physics, Yale University, New Haven, Connecticut 06520, USA*
[2] *Department of Physics, Taras Shevchenko National University of Kyiv, Kyiv, 03022, Ukraine*
[3] *Bogolyubov Institute for Theoretical Physics, Kyiv, 03143, Ukraine*
[4] *College of Integrative Sciences and Arts, Arizona State University, Mesa, Arizona 85212, USA*
[5] *Department of Physics, Arizona State University, Tempe, Arizona 85287, USA*

(Dated: October 21, 2021)

Hydrodynamic instabilities driven by a direct current are analyzed in 2D and 3D relativisticlike systems with the Dyakonov-Shur boundary conditions supplemented by a boundary condition for temperature. Besides the conventional Dyakonov-Shur instability for plasmons, we find an entropy wave instability in both 2D and 3D systems. The entropy wave instability is a manifestation of the relativisticlike nature of electron quasiparticles and a nontrivial role of the energy current in such systems. These two instabilities occur for the opposite directions of fluid flow. While the Dyakonov-Shur instability is characterized by the plasma frequency in 3D and the system size in 2D, the frequency of the entropy wave instability is tunable by the system size and the flow velocity.

Introduction.— Plasma instabilities attract significant attention and play an important role in various branches of science including high-energy and condensed matter physics, astrophysics, controlled thermonuclear fusion, etc. A few decades ago Dyakonov and Shur predicted [1] that an electron plasma in a hydrodynamic regime should become unstable in a biased two-dimensional (2D) heterostructure subject to a background direct current (dc) flow and rather unconventional asymmetric alternating current (ac) boundary conditions. This Dyakonov-Shur instability (DSI) appears due to the amplification of plasma waves (equivalently, plasmons) caused by multiple reflections from the device boundaries. Such an enhancement is reminiscent of the Fermi acceleration mechanism [2, 3], where charged particles are accelerated due to reflection from shock fronts or moving magnetic mirrors. The DSI could provide an effective way to create sources of terahertz radiation by using a direct current. This is particularly important in the modern industry where compact, efficient, and tunable sources of terahertz radiation are needed [4]. Furthermore, the DSI allows one to detect terahertz radiation by converting an ac signal to the dc one [5], which could be used to create terahertz detectors.

The recent surge of interest in the DSI is connected with the experimental observation of the electron hydrodynamics in 2D electron gas of (Al, Ga)As heterostructures [6, 7] and graphene [8–14] (see Refs. [15, 16] for recent reviews on electron hydrodynamics). In addition to 2D systems, evidence of three-dimensional (3D) relativisticlike hydrodynamic electron transport was reported in the Weyl semimetal tungsten diphosphide WP_2 [17]. Because Dirac and Weyl semimetals provide a suitable platform for investigating electron hydrodynamics in solids, the DSI in graphene received a lot of attention [18–22]. Despite extensive theoretical studies, the generation of terahertz waves by the DSI was not confirmed experimentally yet. Nevertheless, the inverse effect, namely the rectification of ac signals, was reported in Refs. [23–27].

Motivated by the recent experimental progress in Dirac and Weyl semimetals, we study hydrodynamic instabilities driven by a dc current in relativisticlike 2D and 3D systems with the Dyakonov-Shur boundary conditions amended by a fixed temperature boundary condition. Since the energy flow can be as important as the charge flow in a relativisticlike system, we pay special attention to the energy current in the hydrodynamic description. One of our main findings is an instability associated with the entropy waves [28, 29]. We dub it the entropy wave instability (EWI). Unlike the conventional DSI, the frequency of the EWI is determined by the flow velocity. This makes the corresponding unstable modes easily tunable. Interestingly, the EWI and DSI occur for the currents of opposite directions.

Model.— In the hydrodynamic regime, the dynamics of the electron fluid made of relativisticlike quasiparticles is described by the Navier-Stokes equation, the charge and energy continuity relations, and the Gauss law that relates the electric potential to the charge density. The corresponding system of equations reads [15, 16]

$$\frac{1}{v_F^2}\left[\partial_t+(\mathbf{u}\cdot\boldsymbol{\nabla})\right](\mathbf{u}w)+\frac{1}{v_F^2}w\mathbf{u}(\boldsymbol{\nabla}\cdot\mathbf{u}) = -\boldsymbol{\nabla}P+en\boldsymbol{\nabla}\varphi+\eta\Delta\mathbf{u}+\eta\frac{d-2}{d}\boldsymbol{\nabla}(\boldsymbol{\nabla}\cdot\mathbf{u})-\frac{w\mathbf{u}}{v_F^2\tau}, \tag{1}$$

$$-e\partial_t n+(\boldsymbol{\nabla}\cdot\mathbf{J})=0, \tag{2}$$

$$\partial_t\epsilon+(\boldsymbol{\nabla}\cdot\mathbf{J}^{\epsilon})=(\mathbf{E}\cdot\mathbf{J}), \tag{3}$$

$$\Delta\varphi=4\pi e\,(n-n_0). \tag{4}$$

Here, $w=\epsilon+P$ is the enthalpy, ϵ is the energy density, P is the pressure, $\mathbf{u}$ is the electron fluid velocity, n is the electron number density, $-e$ is the electron charge, and v_F is the Fermi velocity. Notice that, because of a relativisticlike dispersion of quasiparticles, the thermodynamic quantities depend on the fluid velocity in the

laboratory (ion lattice) frame. Their explicit expressions are given in the Supplemental Material [30]. Unlike other quantities, the equilibrium charge densities in the laboratory and comoving frames are the same (i.e., $n = n_0$), since they must be compensated by the charge density of ions. From general considerations, the hydrodynamic regime is expected to break down when the fluid velocity approaches v_F. Therefore, we will assume that $u \ll v_F$.

In Eq. (1), the shear viscosity η is defined as $\eta = \eta_{\rm kin} w/v_F^2$, where $\eta_{\rm kin}$ is the kinematic shear viscosity [31]. The momentum relaxation is quantified by the relaxation time τ that describes scattering on impurities and phonons. In the hydrodynamic regime, we neglect the intrinsic electric and thermal conductivities [15]. Therefore, the electric and energy current densities are proportional to fluid velocity $\mathbf{u}$, i.e., $\mathbf{J} = -en\mathbf{u}$ and $\mathbf{J}^\epsilon = w\mathbf{u}$.

To study current-driven instabilities, we employ the conventional linear stability analysis where weak fluctuations are superimposed on top of a steady uniform flow, quantified by the fluid velocity $\mathbf{u}_0 = u_0\hat{\mathbf{x}}$, e.g.,

$$u_x(t,\mathbf{r}) = u_0 + u_1 e^{-i\omega t + i\mathbf{k}\cdot\mathbf{r}}. \tag{5}$$

Similar expressions are valid also for the other quantities (n, φ, and ϵ). Here, ω and $\mathbf{k}$ are the angular frequency and the wave vector of excitations, respectively. For the sake of simplicity, we neglect all transverse fluctuations and focus on the one-dimensional instability assuming $\mathbf{k} = k_x\hat{\mathbf{x}}$. Linearizing Eqs. (1)–(4) and using ansatz (5), we obtain the following set of linear algebraic equations at $\eta = 0$:

$$(\omega - 2k_x u_0)\, u_1 + \frac{u_0}{w_0}(\omega - k_x u_0)\, w_1 - k_x \frac{v_F^2}{w_0} P_1 + i\frac{u_0}{\tau}\left(\frac{u_1}{u_0} + \frac{w_1}{w_0} - \frac{n_1}{n_0}\right) = -k_x \frac{e n_0 v_F^2}{w_0}\varphi_1, \tag{6}$$

$$(\omega - k_x u_0)\, n_1 = k_x n_0 u_1, \tag{7}$$

$$\omega\epsilon_1 - k_x u_0 w_1 - k_x w_0 u_1 - i\frac{1}{\tau}\frac{u_0^2}{v_F^2} w_0\left(\frac{n_1}{n_0} + \frac{u_1}{u_0}\right) = -u_0 k_x e n_0 \varphi_1, \tag{8}$$

$$\text{3D:}\quad \varphi_1 = -\frac{4\pi e}{k^2} n_1 \quad \text{or} \quad \text{2D:}\quad \varphi_1 = -\frac{e}{C} n_1. \tag{9}$$

In the 2D system, we use the "gradual channel" approximation [1, 32], where $C = \varepsilon/(4\pi L_g)$ is the capacitance per unit area, ε is the dielectric constant of the substrate, and L_g is the distance to the gate. Note that the steady-state solution of the hydrodynamic equations implies the presence of electric field $E_0 = -w_0 u_0/(e n_0 v_F^2 \tau)$, which was explicitly used in Eqs. (6) and (8).

In the dissipationless limit ($\tau \to \infty$) and to the leading order in $|u_0|/v_F$, the characteristic equation that determines the spectrum of collective modes reads (see Supplemental Material [30] for details)

$$(\omega - u_0 k_x)\left[\omega^2 - \omega_p^2 + u_0 k_x\left(u_0 k_x - \frac{4}{3}\omega\right) - v_s^2 k_x^2\right] = 0 \tag{10}$$

in 3D and

$$(\omega - u_0 k_x)\left[\omega(\omega - u_0 k_x) - v_s^2 k_x^2 (1+\xi)\right] = 0 \tag{11}$$

in 2D. Here, $v_s = v_F/\sqrt{d}$ is the sound velocity in a d-dimensional space ($d = 2, 3$). The square of the plasma frequency for a 3D relativisticlike fluid is given by

$$\omega_p^2 = \frac{4\pi e^2 n_0^2 v_F^2}{w_0}. \tag{12}$$

In the 2D case, we introduced dimensionless parameter $\xi = 2e^2 n_0^2/(w_0 C)$.

Collective modes.— To clarify the physical origin of the EWI, it is instructive to determine the solutions to the characteristic equations (10) and (11) in an infinite medium without imposing any boundary conditions.

To the leading order in $|u_0|/v_F \ll 1$, we find the following dispersion relations for collective modes:

$$\text{3D:}\quad \omega_\pm \approx \pm\sqrt{\omega_p^2 + v_s^2 k_x^2} + \frac{2}{3}u_0 k_x, \tag{13}$$

$$\text{2D:}\quad \omega_\pm \approx \pm v_p k_x + \frac{1}{2}u_0 k_x, \tag{14}$$

$$\text{2D and 3D:}\quad \omega_e \approx u_0 k_x. \tag{15}$$

Here, $\omega_\pm$ correspond to plasmons. Notice that the plasmon spectrum in a gated 2D sample is gapless and linear in the wave vector. The corresponding plasmon velocity is $v_p = v_s\sqrt{1+\xi}$. The third solution ω_e given in Eq. (15) corresponds to the so-called entropy wave [28, 29].

Considering the important role of the entropy wave, let us discuss its properties in detail. For simplicity, we consider the limit $\tau \to \infty$. In drastic contrast to plasmons, the flow velocity does not oscillate in this wave, i.e., $u_1 = 0$. It is characterized by oscillating electron number n_1 and energy ϵ_1 densities and, in turn, the entropy. As follows from the Navier-Stokes equation (6), the solution with $u_1 = 0$ is possible because the gradient of pressure defined by the third term on the left-hand

side of the equation is counterbalanced by the Coulomb force provided by the term on the right-hand side. To the leading order in $|u_0|/v_s$, one finds that

$$\frac{n_1}{n_0} \approx -\left(\frac{v_s k_x}{\omega_p}\right)^2 \frac{\epsilon_1}{w_0}. \tag{16}$$

According to Eq. (15), the entropy wave is a downstream wave; i.e., it propagates with the local flow velocity u_0.

It is interesting to point out that modes with similar dispersion relations appear in geophysics. For example, the Coriolis force and the pressure gradient compensate each other in the Rossby wave [33], which is an inertial wave occurring in rotating fluids. Its dispersion relation contains the term $\propto u_0 k_x$ and a term quadratic in k_x due to the coordinate dependence of the planetary vorticity. In the absence of background flow, the frequency of the entropy mode is zero which is analogous to geostrophic currents [34].

Boundary conditions and instabilities.— Both plasmons and entropy waves are stable collective modes in an infinite medium. Let us show now that the stability of these modes is affected profoundly by the boundary conditions. We consider a sample with length L along the x direction. In addition to the standard Dyakonov-Shur boundary conditions, we fix temperature at the left ($x = 0$) surface

$$n_1(x = 0) = 0, \tag{17}$$

$$J_x(x = L) \equiv n_0 u_1(x = L) + u_0 n_1(x = L) = 0, \tag{18}$$

$$T_1(x = 0) = 0. \tag{19}$$

Physically the Dyakonov-Shur boundary conditions correspond to short circuiting the sample at $x = 0$ (zero impedance) (17) and leaving the other side $x = L$ open (infinite impedance) (18). The condition in Eq. (19) can be enforced by connecting the boundary to a large thermostat, e.g., made of a metal with high thermal conductivity and specific heat.

It is convenient to solve hydrodynamic equations in terms of u_1, n_1, and ϵ_1. One can show (see Supplemental Material [30] for details) that oscillations of pressure P_1 are related to ϵ_1 as follows:

$$P_1 \approx \frac{\epsilon_1}{d} - \epsilon_0 \frac{2(d+1)}{d^3} \frac{u_1 u_0}{v_s^2}, \tag{20}$$

at the leading order in $|u_0|/v_s$. Then, the boundary condition (19) can be reexpressed in terms of ϵ_1 and u_1, i.e.,

$$\epsilon_1(x = 0) \approx \frac{u_1 u_0}{v_s^2} \frac{d+1}{d^2} \epsilon_0 \left[1 - (d+1)\left(1 - \Lambda_p^2\right)\right], \tag{21}$$

where $\Lambda_p = \omega_p/(v_s q_{\mathrm{TF}})$ and $q_{\mathrm{TF}}^2 = 4\pi e^2 (\partial_\mu n_0)$ is the square of the Thomas-Fermi wave vector.

We seek solutions to Eqs. (6)–(9) in the form

$$\frac{n_1}{n_0} = \sum_{j=1}^{3} C_j e^{i k_j x} \tag{22}$$

and define u_1, ϵ_1, and φ_1 from Eqs. (7)–(9) (see Supplemental Material [30] for the corresponding expressions). Here, $\sum_j$ runs over the three roots $k_j(\omega)$ of Eq. (10) or (11). By using the boundary conditions (17), (18), and (21), we derive the characteristic equation for ω, which defines allowed collective modes in the system.

Let us start with the plasmons. To the linear order in u_0, their frequencies are given by the following relations:

$$\omega_{\pm}^{3D} \approx \pm\sqrt{\omega_p^2 + \left[v_s \frac{\pi}{L}\left(l + \frac{1}{2}\right)\right]^2} + i\frac{2u_0}{3L}\left(3 - 2\Lambda_p^2\right) \tag{23}$$

in the 3D case, and

$$\omega_{\pm}^{2D} \approx \pm v_p \frac{\pi}{L}\left(l + \frac{1}{2}\right) + i\frac{u_0}{2L}\left(4 - 3\Lambda_p^2\right) \tag{24}$$

in the 2D case, respectively. In both expressions, $l \in \mathbb{Z}$. (For the results to the quadratic order in u_0, see SM.) Since $0 < \Lambda_p < 1$ for $T \neq 0$ (see SM for the temperature dependence of Λ_p), the plasmons are unstable in both 3D and 2D systems. This is in agreement with Refs. [19, 22] for slow flow [35].

As we see from Eqs. (23) and (24), enforcing the boundary conditions leads to the DSI for $u_0 > 0$. In the linear regime, it is quantified by a growing amplitude $\propto e^{\mathrm{Im}[\omega_\pm]t}$. Eventually, the growth will be cut off by nonlinearities (see, e.g. Refs. [21, 22]). As for the real part, the plasmon frequencies are quantized due to the finite thickness of the slab, where $k_x \to \pi(l+1/2)/L$. As expected, the minimal frequency is determined by ω_p in 3D and the inverse sample size in 2D.

Entropy wave instability and numerical results.— Let us turn to the entropy mode now. By solving the characteristic equation for large $L\omega_p/v_s$ [36], the corresponding frequency can be approximated as

$$\omega_e^{3D} \approx \frac{2\pi l}{L} u_0 - i\frac{u_0 \omega_p}{v_s} - i\frac{u_0}{L} \ln\left[\frac{3}{8} \frac{v_s^2}{u_0^2\left(1 - \Lambda_p^2\right)}\right] \tag{25}$$

in 3D and

$$\omega_e^{2D} \approx \frac{2\pi l}{L} u_0 - i\frac{u_0}{L} \ln\left[\frac{2}{3} \frac{v_p^2}{u_0^2\left(1 - \Lambda_p^2\right)}\right] \tag{26}$$

in 2D. For the entropy wave, unlike plasmons, the real part of ω_e is controlled by the flow velocity and the sample size, i.e., $\mathrm{Re}\,[\omega_e] \propto u_0/L$, in both 2D and 3D. The entropy mode becomes unstable for $u_0 < 0$ due to the combined effect of the fluid flow and the boundary conditions.

Let us emphasize several distinctions between the plasmon and entropy modes. Plasmons are characterized by large in-phase oscillations of energy and number densities, as well as having a non-negligible velocity (see Supplemental Material [30] for details). They are also delocalized; i.e., the magnitude of oscillations is large

throughout the slab. In the case of entropy modes, oscillations of velocity are suppressed. Unlike plasmons, these modes show a noticeable localization at the $x = L$ interface. This localization becomes less pronounced for the modes with large l when the real part $|\mathrm{Re}\,[\omega_e]\,| \gtrsim \omega_p$ in 3D or $|\mathrm{Re}\,[\omega_e]\,| \gtrsim v_s\pi/(2L)$ in 2D, when the entropy waves may hybridize with plasmons.

Our numerical and approximate analytical results for collective modes in a 3D Dirac system are shown in Fig. 1. The results for the 2D case are qualitatively similar with the frequency scale normalized by v_s/L instead of ω_p (see Supplemental Material [30]). The separation between the branches of both modes become small for realistic system size $L\omega_p/v_s \gg 1$. While this complicates the numerical calculations and obscures the presentation, the qualitative features remain the same as for $L\omega_p/v_s \sim 10$. Therefore, for the sake of clarity, we use a rather small width $L = 10\,v_s/\omega_p$ and show only the lowest five branches of the numerical results and the approximate analytical solutions given in Eq. (25). As one can see, even at such a small width, the density of solutions quickly increases at $u_0 \to 0$ for the entropy mode. It is clear from Fig. 1 that the approximate expressions (23) and (25) agree well with the numerical results. As expected, the plasmons have nonzero frequencies at $u_0 \to 0$ and the solutions for the entropy modes vanish in this limit. We notice also that the instability increment is much larger for the entropy waves than for plasmons. Therefore, the corresponding instability should be more pronounced than the DSI for the same flow velocities.

All in all, different frequencies, growth rates, and spatial profiles of oscillating variables make the EWI profoundly different from the conventional DSI.

Estimates and momentum relaxation effects.— For typical 3D Dirac and Weyl semimetal parameters, we use $\mu_0 = 20$ meV, $T_0 = 25$ K, and the Fermi velocity $v_F \approx 1.4 \times 10^7$ cm/s [37]. Then, we estimate $\omega_p/(2\pi) \approx 12$ THz and $v_s \approx 8 \times 10^6$ cm/s. The characteristic length scale is $v_s/\omega_p \approx 1$ nm.

For the 2D case, we use graphene as a characteristic system with $v_F = 1.1 \times 10^8$ cm/s, $\mu_0 = 100$ meV, $T_0 = 100$ K, $L_g = 100$ nm, and $\varepsilon = 3.3$ (assuming a hexagonal boron nitride substrate). In this case, $v_s \approx 7.8 \times 10^7$ cm/s, $\xi \approx 65.1$, and $v_p \approx 8.1\,v_s$. The corresponding characteristic frequency of collective modes is $v_p/L \approx (1\ \mu\mathrm{m}/L)$ THz, i.e., it also lies in the terahertz range.

It is instructive to discuss briefly the effects of momentum relaxation and viscosity. In view of a distinct nature of plasmons and entropy waves, the role of momentum relaxation in the DSI and EWI is qualitatively different. The suppression of the plasmon DSI can be roughly described by replacing $\omega \to \omega - i/\tau$, where τ is the relaxation time. For the parameters used, the instability disappears when $\tau \lesssim 3L/(2u_0)$ in 3D and $\tau \lesssim 2L/u_0$ in 2D (we assumed $\Lambda_p \approx 1$ here). On the other hand,

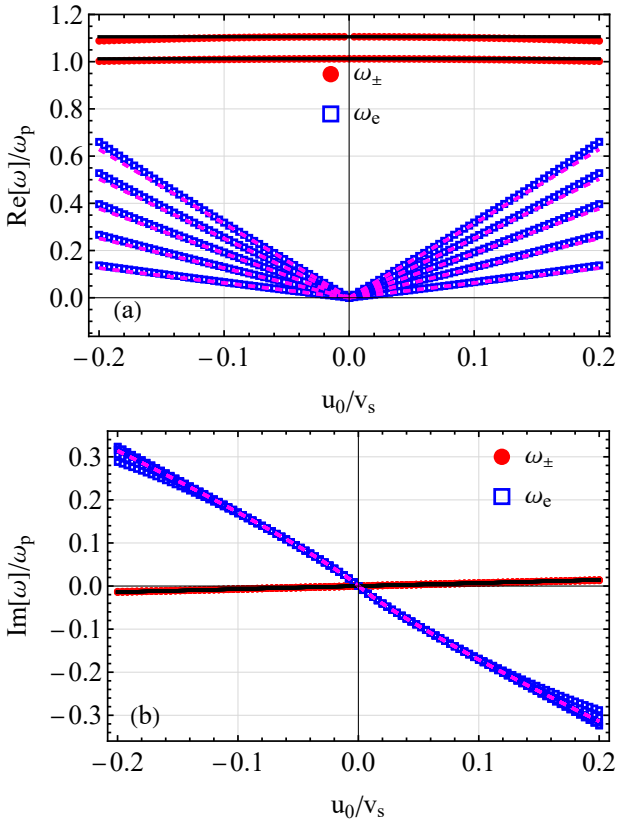

FIG. 1. The real (a) and imaginary (b) parts of the frequency of collective modes as a function of velocity u_0 in the 3D case. We show only the lowest five branches of numerical and approximate analytical results. Black solid lines correspond to the approximate expression (23). The approximate relation (25) is shown by magenta dashed lines. We fixed $L = 10\,v_s/\omega_p$, $\Lambda_p \approx 0.98$, and took the limit $\tau \to \infty$.

the EWI is quite robust with respect to momentum relaxation. This is explained by the fact that these waves have weak oscillating velocity compared to other oscillating variables, e.g., $|u_1|/v_s \ll |n_1|/n_0$; see also Supplemental Material. The effects of viscosity can be estimated similar to Ref. [1] as $\omega - i/\tau \to \omega - i/\tau - i\eta_{\mathrm{kin}}\pi^2/L^2$. In essence, it also suppresses the DSI but becomes important only for a small width. A more detailed study of the dissipation effects will be reported elsewhere.

Summary.— We found that Dirac and Weyl semimetals, subject to the Dyakonov-Shur boundary conditions and a boundary condition for temperature, develop an entropy wave instability. The latter is connected with the entropy mode in relativisticlike hydrodynamics, where the energy current plays an important role. The entropy wave instability is absent in materials with a nonrelativistic energy dispersion, where the energy current plays a secondary role.

We estimate that the growth rate of the entropy wave instability is parametrically larger than that for the Dyakonov-Shur instability. Moreover, the two instabil-

ities occur for the opposite directions of the applied current. The frequencies of unstable modes are determined by the system size and the flow velocity (entropy wave), only the system size (2D plasmons), and the plasmon frequency (3D plasmons). The tunability of the entropy wave instability provides the means to detect and distinguish it from other instabilities in the experiment. It can be identified by measuring the emission of radiation with a frequency proportional to the flow velocity. Our estimates suggest that the current-driven instabilities are achievable for realistic samples and flow velocities. Thus, the entropy wave instability holds a potential for use in tunable sources of radiation.

We are grateful to Dmitry Svintsov for bringing our attention to the problem of the DSI in 3D systems and for useful discussions. P.O.S. acknowledges the support through the Yale Prize Postdoctoral Fellowship in Condensed Matter Theory. The work of I.A.S. was supported by the U.S. National Science Foundation under Grant No. PHY-1713950.

* pavlo.sukhachov@yale.edu

[1] M. Dyakonov and M. Shur, Shallow water analogy for a ballistic field effect transistor: New mechanism of plasma wave generation by dc current, Phys. Rev. Lett. **71**, 2465 (1993).

[2] G. F. Krymskii, A regular mechanism for the acceleration of charged particles on the front of a shock wave, Sov. Phys. - Dokl. **22**, 327 (1977).

[3] A. R. Bell, The acceleration of cosmic rays in shock fronts – I, Mon. Not. R. Astron. Soc. **182**, 147 (1978).

[4] S. S. Dhillon, M. S. Vitiello, E. H. Linfield, A. G. Davies, M. C. Hoffmann, J. Booske, C. Paoloni, M. Gensch, P. Weightman, G. P. Williams, E. Castro-Camus, D. R. Cumming, F. Simoens, I. Escorcia-Carranza, J. Grant, S. Lucyszyn, M. Kuwata-Gonokami, K. Konishi, M. Koch, C. A. Schmuttenmaer, T. L. Cocker, R. Huber, A. G. Markelz, Z. D. Taylor, V. P. Wallace, J. Axel Zeitler, J. Sibik, T. M. Korter, B. Ellison, S. Rea, P. Goldsmith, K. B. Cooper, R. Appleby, D. Pardo, P. G. Huggard, V. Krozer, H. Shams, M. Fice, C. Renaud, A. Seeds, A. Stöhr, M. Naftaly, N. Ridler, R. Clarke, J. E. Cunningham, and M. B. Johnston, The 2017 terahertz science and technology roadmap, J. Phys. D. Appl. Phys. **50**, 043001 (2017).

[5] M. Dyakonov and M. Shur, Detection, mixing, and frequency multiplication of terahertz radiation by two-dimensional electronic fluid, IEEE Trans. Electron Dev. **43**, 380 (1996).

[6] L. W. Molenkamp and M. J. de Jong, Observation of Knudsen and Gurzhi transport regimes in a two-dimensional wire, Solid State Electron. **37**, 551 (1994).

[7] M. J. M. De Jong and L. W. Molenkamp, Hydrodynamic electron flow in high-mobility wires, Phys. Rev. B **51**, 13389 (1995).

[8] J. Crossno, J. K. Shi, K. Wang, X. Liu, A. Harzheim, A. Lucas, S. Sachdev, P. Kim, T. Taniguchi, K. Watanabe, T. A. Ohki, and K. C. Fong, Observation of the Dirac fluid and the breakdown of the Wiedemann-Franz law in graphene, Science **351**, 1058 (2016).

[9] F. Ghahari, H.-Y. Xie, T. Taniguchi, K. Watanabe, M. S. Foster, and P. Kim, Enhanced Thermoelectric Power in Graphene: Violation of the Mott Relation by Inelastic Scattering, Phys. Rev. Lett. **116**, 136802 (2016).

[10] R. Krishna Kumar, D. A. Bandurin, F. M. D. Pellegrino, Y. Cao, A. Principi, H. Guo, G. H. Auton, M. Ben Shalom, L. A. Ponomarenko, G. Falkovich, K. Watanabe, T. Taniguchi, I. V. Grigorieva, L. S. Levitov, M. Polini, and A. K. Geim, Superballistic flow of viscous electron fluid through graphene constrictions, Nat. Phys. **13**, 1182 (2017).

[11] A. I. Berdyugin, S. G. Xu, F. M. D. Pellegrino, R. Krishna Kumar, A. Principi, I. Torre, M. Ben Shalom, T. Taniguchi, K. Watanabe, I. V. Grigorieva, M. Polini, A. K. Geim, and D. A. Bandurin, Measuring Hall viscosity of graphene's electron fluid, Science **364**, 162 (2019).

[12] D. A. Bandurin, A. V. Shytov, L. S. Levitov, R. K. Kumar, A. I. Berdyugin, M. Ben Shalom, I. V. Grigorieva, A. K. Geim, and G. Falkovich, Fluidity onset in graphene, Nat. Commun. **9**, 4533 (2018).

[13] M. J. H. Ku, T. X. Zhou, Q. Li, Y. J. Shin, J. K. Shi, C. Burch, L. E. Anderson, A. T. Pierce, Y. Xie, A. Hamo, U. Vool, H. Zhang, F. Casola, T. Taniguchi, K. Watanabe, M. M. Fogler, P. Kim, A. Yacoby, and R. L. Walsworth, Imaging viscous flow of the Dirac fluid in graphene, Nature (London) **583**, 537 (2020).

[14] J. A. Sulpizio, L. Ella, A. Rozen, J. Birkbeck, D. J. Perello, D. Dutta, M. Ben-Shalom, T. Taniguchi, K. Watanabe, T. Holder, R. Queiroz, A. Principi, A. Stern, T. Scaffidi, A. K. Geim, and S. Ilani, Visualizing Poiseuille flow of hydrodynamic electrons, Nature (London) **576**, 75 (2019).

[15] A. Lucas and K. C. Fong, Hydrodynamics of electrons in graphene, J. Phys. Condens. Matter **94**, 2280 (2017).

[16] B. N. Narozhny, Electronic hydrodynamics in graphene, Ann. Phys. (Amsterdam)) **411**, 167979 (2019).

[17] J. Gooth, F. Menges, N. Kumar, V. Süβ, C. Shekhar, Y. Sun, U. Drechsler, R. Zierold, C. Felser, and B. Gotsmann, Thermal and electrical signatures of a hydrodynamic electron fluid in tungsten diphosphide, Nat. Commun. **9**, 4093 (2018).

[18] A. Tomadin and M. Polini, Theory of the plasma-wave photoresponse of a gated graphene sheet, Phys. Rev. B **88**, 205426 (2013).

[19] D. Svintsov, V. Vyurkov, V. Ryzhii, and T. Otsuji, Hydrodynamic electron transport and nonlinear waves in graphene, Phys. Rev. B **88**, 245444 (2013).

[20] Y. Koseki, V. Ryzhii, T. Otsuji, V. V. Popov, and A. Satou, Giant plasmon instability in a dual-grating-gate graphene field-effect transistor, Phys. Rev. B **93**, 245408 (2016).

[21] C. B. Mendl, M. Polini, and A. Lucas, Coherent terahertz radiation from a nonlinear oscillator of viscous electrons, Appl. Phys. Lett. **118**, 013105 (2021).

[22] J. Crabb, X. Cantos-Roman, J. M. Jornet, and G. R. Aizin, Hydrodynamic theory of the Dyakonov-Shur instability in graphene transistors (2021), arXiv:2106.01296.

[23] R. Tauk, F. Teppe, S. Boubanga, D. Coquillat, W. Knap, Y. M. Meziani, C. Gallon, F. Boeuf, T. Skotnicki, C. Fenouillet-Beranger, D. K. Maude, S. Rumyantsev, and M. S. Shur, Plasma wave detection of terahertz radiation by silicon field effects

transistors: Responsivity and noise equivalent power, Appl. Phys. Lett. **89**, 253511 (2006).
[24] M. S. Vitiello, D. Coquillat, L. Viti, D. Ercolani, F. Teppe, A. Pitanti, F. Beltram, L. Sorba, W. Knap, and A. Tredicucci, Room-temperature terahertz detectors based on semiconductor nanowire field-effect transistors, Nano Lett. **12**, 96 (2012).
[25] L. Vicarelli, M. S. Vitiello, D. Coquillat, A. Lombardo, A. C. Ferrari, W. Knap, M. Polini, V. Pellegrini, and A. Tredicucci, Graphene field effect transistors as room-temperature terahertz detectors, Nat. Mater. **11**, 865 (2012).
[26] V. Giliberti, A. Di Gaspare, E. Giovine, M. Ortolani, L. Sorba, G. Biasiol, V. V. Popov, D. V. Fateev, and F. Evangelisti, Downconversion of terahertz radiation due to intrinsic hydrodynamic nonlinearity of a two-dimensional electron plasma, Phys. Rev. B **91**, 165313 (2015).
[27] D. A. Bandurin, I. Gayduchenko, Y. Cao, M. Moskotin, A. Principi, I. V. Grigorieva, G. Goltsman, G. Fedorov, and D. Svintsov, Dual origin of room temperature subterahertz photoresponse in graphene field effect transistors, Appl. Phys. Lett. **112**, 141101 (2018).
[28] L. D. Landau and E. M. Lifshitz, *Fluid Mechanics* (Butterworth-Heinemann, Oxford, 2013).
[29] G. I. Ogilvie, Astrophysical fluid dynamics, J. Plasma Phys. **82**, 205820301 (2016).
[30] See Supplemental Material for details of the derivations of thermodynamic variables, boundary conditions, solutions for the hydrodynamic deviations, and frequencies of plasmons and entropy modes in graphene. The Supplemental Material contains Refs. [38–40].
[31] The bulk viscosity is vanishingly small in systems with relativisticlike quasiparticles, see, e.g., Ref. [41] for an explicit calculation in graphene.
[32] M. S. Shur, *GaAs Devices and Circuits* (Springer US, New York, 1987).
[33] C.-G. Rossby, Relation between variations in the intensity of the zonal circulation of the atmosphere and the displacements of the semi-permanent centers of action, J. Mar. Res. **2**, 38 (1939).
[34] A. Gill, *Atmosphere-Ocean Dynamics* (Academic Press, New York, 1982).
[35] The growth rate for plasmons (14) differs from that in Ref. [18]. The discrepancy can be traced to a different form of the nonlinear terms in the Navier-Stokes equation and the dependence of pressure P on velocity.
[36] The hydrodynamic description is invalid for $L\omega_p/v_s \lesssim 1$ because the system size becomes comparable to the intercarrier distance in this case.
[37] N. Kumar, Y. Sun, N. Xu, K. Manna, M. Yao, V. Süss, I. Leermakers, O. Young, T. Förster, M. Schmidt, H. Borrmann, B. Yan, U. Zeitler, M. Shi, C. Felser, and C. Shekhar, Extremely high magnetoresistance and conductivity in the type-II Weyl semimetals WP_2 and MoP_2, Nat. Commun. **8**, 1642 (2017).
[38] V. F. Gantmakher and Y. B. Levinson, *Carrier scattering in metals and semiconductors*, Modern problems in condensed matter sciences (North-Holland, Amsterdam, 1987).
[39] E. V. Gorbar, V. A. Miransky, I. A. Shovkovy, and P. O. Sukhachov, Consistent hydrodynamic theory of chiral electrons in Weyl semimetals, Phys. Rev. B **97**, 121105(R) (2018).
[40] S. H. Abedinpour, G. Vignale, A. Principi, M. Polini, W.-K. Tse, and A. H. MacDonald, Drude weight, plasmon dispersion, and ac conductivity in doped graphene sheets, Phys. Rev. B **84**, 045429 (2011).
[41] A. Principi, G. Vignale, M. Carrega, and M. Polini, Bulk and shear viscosities of the two-dimensional electron liquid in a doped graphene sheet, Phys. Rev. B **93**, 125410 (2016).